

## Article

# Research on the Characteristics of Urban Building Cluster Wind Field Based on UAV Wind Measurement

Ou Pu <sup>1,2,\*</sup>, Boqiu Yuan <sup>1</sup>, Zhengnong Li <sup>3</sup>, Terigen Bao <sup>3</sup>, Zheng Chen <sup>4</sup>, Liwei Yang <sup>1</sup>, Hua Qin <sup>1</sup> and Zhen Li <sup>1</sup>

<sup>1</sup> Power Grid Planning Research Center, Guangxi Power Grid Co., Ltd., Nanning 530023, China; qin\_h@gx.csg.cn (H.Q.); li\_z@im.gx.csg (Z.L.)

<sup>2</sup> Postdoctoral Research Workstation, Guangxi Power Grid Co., Ltd., Nanning 530023, China

<sup>3</sup> Key Laboratory of Building Safety and Energy Efficiency of the Ministry of Education, Hunan University, Changsha 410082, China; lizn@hnu.edu.cn (Z.L.)

<sup>4</sup> School of Civil Engineering and Architecture, State Key Laboratory of Featured Metal Materials and Life-Cycle Safety for Composite Structures, Guangxi University, Nanning 530004, China; chenzheng@gxu.edu.cn

\* Correspondence: puou666@126.com; Tel.: +86-18569053616

**Abstract:** An innovative approach for measuring wind fields in urban building clusters using Unmanned Aerial Vehicles (UAVs) is presented. This method captures the distribution of wind fields within clusters. The results indicate that building architecture has a significant influence on wind flow characteristics at 15 m and 25 m height levels. Particularly, areas adjacent to the buildings and the wake section exhibit notable variations in wind speed and turbulence intensity compared to the incoming flow. The regions most affected include the areas flanking the buildings on either side and the intermediate section of the wake. The flow separation and convergence of incoming wind from the windward sides of the buildings notably amplify the wind load, resulting in a significant shift in wind speed and turbulence intensity within pedestrian pathways. The use of UAVs for wind measurements enables a flexible and efficient assessment of urban wind fields. These findings pave the way for further research into wind field measurements in urban architecture and a better understanding of the interference effects of buildings.

**Keywords:** field measurement; building wake flow; UAV wind measurement system; surface roughness index; wind field characteristics



**Citation:** Pu, O.; Yuan, B.; Li, Z.; Bao, T.; Chen, Z.; Yang, L.; Qin, H.; Li, Z. Research on the Characteristics of Urban Building Cluster Wind Field Based on UAV Wind Measurement. *Buildings* **2023**, *13*, 3109. <https://doi.org/10.3390/buildings13123109>

Academic Editor: Bo Hong

Received: 30 October 2023

Revised: 24 November 2023

Accepted: 12 December 2023

Published: 14 December 2023



**Copyright:** © 2023 by the authors. Licensee MDPI, Basel, Switzerland. This article is an open access article distributed under the terms and conditions of the Creative Commons Attribution (CC BY) license (<https://creativecommons.org/licenses/by/4.0/>).

## 1. Introduction

The modernization progress has led to densely populated urban centers filled with buildings. This has given rise to flow separation, vortex generation, and wind acceleration effects as wind navigates through these structures, causing discomfort in the local wind environment [1]. Therefore, it is crucial to examine the fluctuations in the wind field around buildings. The insights gained from this examination can guide the design of wind-resistant architecture and improve the surrounding wind environment. In densely populated urban areas, buildings readily induce wind field interference effects [2], resulting in significantly different wind loads on structures compared to isolated buildings. These interference effects are influenced by various factors, including the position of the buildings in the urban plan [3], their height [4], the type of terrain [5], and their cross-section [6]. Despite the innate complexity and multivariate traits of interference effects, and the prevalent assumption of ubiquitous shielding effects from neighboring structures, there remains a lack of extensive guidelines, predominantly due to the shortage of comprehensive field experimental data [7–9]. For example, on 18 May 2021, the SEG Plaza in Shenzhen, China, experienced noticeable swaying even under mild wind conditions, drawing significant public attention. The building, standing at 355.8 m, swayed noticeably despite clear weather, no rainfall, and moderate winds (southerly winds at level 3, with maximum

gusts at level 5). Such swaying greatly affected the structural comfort and caused panic among people fearing potential building collapse. The industry generally believes that the swaying was caused by wind effects. Under various factors such as wind speed, temperature, and subway operations, the complex wind environment created Karman vortex streets. The alternating shedding of these vortices, coinciding in frequency with the structure's frequency, triggered structural resonance, leading to the building's swaying. Currently, the wind field undergoes varying degrees of disturbance after passing through dense high-rise buildings, making the urban wind environment extremely complex. This incident highlights the lack of measurement methods to obtain actual inflow wind field conditions, preventing in-depth research into such events. Additionally, it indirectly shows that the results of wind tunnel tests and numerical simulations are still relatively idealized, necessitating the use of on-site measurements for analysis.

Over the past few decades, the wind field of building clusters and their mutual interactions have garnered increased attention, with clarifications pursued via experimental measurements [10,11]. Currently, widely used research methods include wind tunnel tests and numerical simulations. Zhou Yu et al. [12] conducted a study on the mutual interference and wake diffusion of cylinders with the same diameter. They analyzed flow characteristics, including the Reynolds number effect. Lankadasu et al. [13] performed simulations to investigate the flow characteristics around two identical square cylinders. They studied the effects of cylinder spacing and the shear parameter "k" on the Strouhal numbers and aerodynamic characteristics. Mahbub et al. [14] conducted wind tunnel tests to explore the mutual interference effects of two square cylinders arranged side by side. They identified four different flow states based on flow characteristics and found significant differences in the interference effects between square and circular cross-sections due to variations in separation and attachment flow characteristics. Sohankar [15] conducted comprehensive numerical studies on the interference effects of tandem square cylinders in turbulent flows. They covered a range of Reynolds numbers from  $10^3$  to  $10^5$  using Large Eddy Simulation (LES). Their research provided accurate solutions to the Navier–Stokes equations and involved the calculation and analysis of parameters such as vorticity, wind pressure distribution, aerodynamic coefficients, and Reynolds numbers under different spacing conditions.

Due to the existence of mutual interference effects, the detailed standards for wind-resistant design of building structures are still not fully developed, and wind tunnel tests remain an important research method for urban structural wind-resistant design. Sumner et al. [16] measured the flow around two cylinders of the same diameter in a wind tunnel, including the mean aerodynamic forces, vortex-induced vibration, and vortex shedding frequency, and found that the configurations could be roughly categorized as close spacing ( $P/D < 1.5$ ) and moderate spacing ( $1.5 \leq P/D$ ). Li, Li, and Ju [17] investigated the wind interference effects on a typical tall building through wind tunnel tests. Their study revealed significant shielding and channeling effects in wind interference, with dramatic changes in wind pressure coefficients on the side and leeward walls of an upstream building when its wake boundary is interfered with. Taniike [18] demonstrated that the sharp increase in wind load and its response is caused by lower surrounding buildings, emphasizing the need for further research on the interference effects of buildings with varying heights on the surrounding wind field. Gowda et al. [19] conducted a study on the influence of interference effects on the wind pressure distribution of primary structures by arranging square surrounding buildings in parallel. Their results indicated that the interference effects become more severe as the height of the surrounding buildings increases. Furthermore, even when there is a significant distance between two buildings, interference effects still persist. Hui et al. [6] utilized Particle Image Velocimetry (PIV) tests and wind tunnel experiments to investigate the interference effects between two buildings. They revealed that under the influence of interference effects, the peak wind pressure on buildings is 50% higher compared to the case of isolated buildings.

While numerical simulations and wind tunnel tests are the primary methods for studying building wind fields and interference effects, these approaches come with inherent limitations. Numerical simulations require theoretical model validation against experimental data and substantial computational power for large-scale flow field simulations. Wind tunnel tests, due to their experimental constraints, often struggle to meet Reynolds number similarity criteria. Given the complexity of atmospheric wind fields and the tendency toward idealized conditions in simulations and tests, field measurements remain essential for verifying the accuracy of these results.

Traditional on-site wind measurement methods include wind towers [18], LiDARs for wind profiling [19], wind profilers [20], and radiosondes [21,22]. Among these methods, wind towers are commonly used for near-ground static flow field measurements but have limitations in terms of mobility and height, rendering them unsuitable for measuring flow fields within clusters of buildings. Wind profilers and LiDARs operate based on radio and optical reflection principles, respectively, providing broad coverage for measurements. However, they are significantly influenced by algorithms, temperature, and humidity, and they have limited mobility, making them suitable for measurements in fixed-area spatial flow fields. Radio sounding instruments are designed for high-altitude measurements, and commonly used carriers include tethered balloons, airships, fixed-wing UAV measurement systems, and multirotor UAV measurement systems. Balloon and airship measurements are affected by high-altitude winds, and their trajectories are generally uncontrollable, making them suitable for rough measurements of spatial flows. In contrast, multirotor and fixed-wing UAV measurement systems offer better maneuverability and controllable positioning, making them suitable for real-time measurements in large-scale spatial flows. Among UAV measurement systems, both fixed-wing UAV systems [23,24] and multirotor systems [25,26] are utilized. Fixed-wing UAV measurement systems provide advantages such as wide coverage and longer endurance, making them suitable for large-scale flow field measurements. However, they have lower spatial resolution in wind measurements, more sources of error, and cannot hover in the air, making it challenging to perform precise measurements at different locations within a space. On the other hand, multirotor UAV wind measurement systems employ directly mounted anemometers for wind speed measurements [27] and algorithms such as triangle solving for wind speed measurements. These systems offer real-time measurements with high accuracy. Prudden, S. et al. [28,29] analyzed the accuracy of wind speed measurements using a pressure-based anemometer system mounted on a multirotor UAV, highlighting the feasibility of conducting average wind speed and turbulence intensity measurements using multirotor UAVs in hovering mode. This provides theoretical foundations for the installation and measurement of pressure-based anemometers. Tamino Wetz et al. [30] measured atmospheric boundary layer flows using a multirotor UAV system and validated the results using wind towers and Doppler LiDARs, demonstrating that the wind profiles obtained from the two devices are essentially consistent.

In urban environments, traditional wind field measurement methods face numerous challenges and limitations. Firstly, traditional tools like anemometer towers are often limited by their installation height, making it difficult to accurately measure wind speeds at high-rise buildings. Additionally, their fixed location limits spatial resolution, preventing effective capture of complex wind field variations between urban building clusters. Secondly, these methods lack mobility and adaptability in the variable urban environment, making it challenging to quickly and flexibly measure wind fields in different areas and to adapt to rapid changes such as the construction or demolition of buildings. Moreover, environmental factors like building layout, street direction, and surrounding terrain impact the urban wind field, making it difficult for traditional methods to accurately capture the effects of these complex factors. Technology and cost are also major constraints. Although advanced equipment like LiDAR can provide higher measurement accuracy, its high cost and technical requirements limit its widespread application in urban environments. Finally, traditional methods have limitations in terms of data timeliness and continuity. For exam-

ple, anemometer towers can provide continuous data but may not reflect rapid changes in the wind field in real time, while LiDAR can provide real-time data but has high costs and technical requirements for continuous operation. Therefore, exploring new measurement methods, such as using Unmanned Aerial Vehicles (UAVs) for wind field measurement, is an important direction for urban wind field research. It not only improves mobility and spatial resolution but also better adapts to the complexity and variability of the urban environment. When measuring wind speed with UAVs, fixed-wing UAVs are suitable for large-scale measurements and high-speed flight but have limitations in precise positioning and low-speed flight, particularly when detailed measurements of specific areas are needed. While they are adept at covering extensive areas, fixed-wing UAVs struggle to rapidly acquire wind speed profiles, often only providing a general overview of the wind field. On the other hand, multirotor UAVs offer better hovering and precise positioning capabilities, which can alleviate some difficulties in capturing detailed wind profiles. However, to make the data more meaningful, simultaneous measurements using multiple devices are often necessary. Despite their advantages, both fixed-wing and multirotor UAVs have limitations that need to be addressed through further research. Multirotor UAVs, for instance, have poorer stability in strong wind conditions and limited endurance and coverage range. Additionally, the rotors of multirotor UAVs may cause airflow interference with wind speed instruments. Data processing requires precise techniques, and factors such as the operator's skills and varying flight conditions, including wind speed and weather, significantly impact the accuracy of the results. Therefore, even with their respective strengths, both types of UAVs present challenges that necessitate ongoing research and analysis to optimize their use in wind field measurements. The use of UAVs for aerial wind field measurements is a valuable method due to its low cost, maneuverability, and the ability to continuously detect large areas. It can serve as a complementary approach to conventional wind measurement or radar wind measurement to a certain extent.

In this research, we developed a wind field measurement approach using UAVs equipped with ultrasonic anemometers. To meet the requirements of modern measurement technologies, we introduced a dual UAV wind measurement scheme and applied it for field measurements within a designated urban building cluster. These hands-on measurements revealed the inherent traits of the wind field distribution in that specific area. Significantly, this UAV-based methodology presents an innovative approach to assess wind field characteristics in urban structures and the broader urban wind resources. In summary, the results of this research provide new perspectives and in-depth insights into the measurement and understanding of urban wind field characteristics.

## 2. The UAV Anemometry System

The wind measurement system, based on UAV technology, is detailed in Figure 1. This system consists of key components, including a UAV, a high-precision ultrasonic anemometer, an efficient compact radio transmitter, and a laptop for data reception and processing. The chosen UAV model is the DJI M600PRO, a robust hexacopter with dimensions measuring  $1688 \times 1518 \times 553$  mm. Due to its payload capacity of nearly 6 kg, the anemometer is strategically positioned on it. This UAV is notable for its operational range of up to 3.5 km and impressive vertical and horizontal precision of  $\pm 0.5$  m. It boasts a flight duration of approximately 30 min and can maintain stable flight even in wind conditions of up to 17 m/s. Upon ascent, the UAV establishes a secure wireless connection with the ground laptop using the compact radio transmitter, enabling real-time data transmission. For the collection of horizontal wind speed data, the UAV is equipped with a 2D ultrasonic anemometer, specifically the SA210 model. The installation position of the ultrasonic anemometer SA210 was determined through the research group's preliminary wind tunnel experiments [31]. The anemometer was mounted 20 cm above the center of the UAV's body, which is identified as the position where the influence of the UAV's rotor airflow on the incoming wind field is minimal. With the necessary circuit modifications, the anemometer

is powered directly by the UAV. Detailed specifications of the anemometer can be found in Table 1.

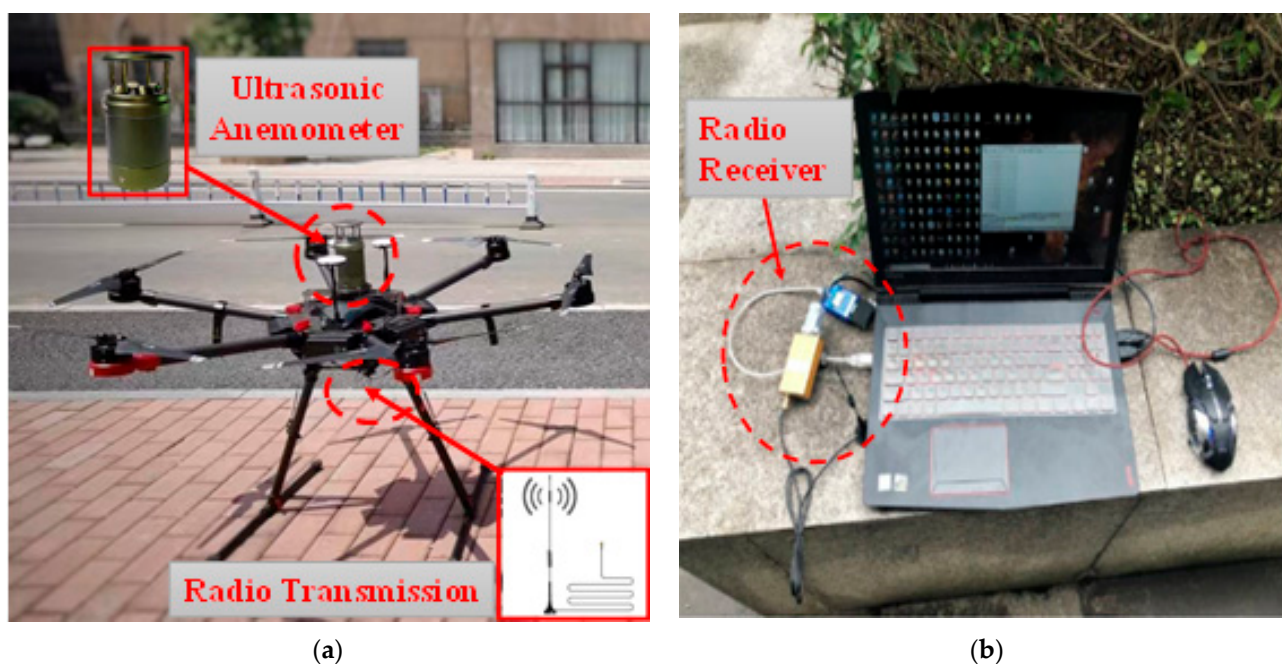


**Figure 1.** The UAV wind measurement system: (a) The hexacopter; (b) The laptop.

**Table 1.** Key specifications of the anemometer.

| Model | Wind Speed Range | Wind Direction Range | Resolution                                 | Measurement Accuracy  | Sampling Rate | Dimensions  | Weight |
|-------|------------------|----------------------|--|---|---------------|---|--------|
| SA210 | 0–50 m/s         | 0–360°               | Wind speed: 0.1 m/s;<br>Wind direction: 1° | Wind speed: 0.5 m/s (0–10 m/s), $\pm 5\%$ (10–50 m/s);<br>Wind direction: $\pm 4^\circ$ | 1 Hz          | $\varnothing 73 \text{ mm} \times 157.5 \text{ mm}$ | 0.5 kg |

It is important to note that when measuring wind fields in urban building clusters using Unmanned Aerial Vehicles (UAVs), in addition to flight height and safety restrictions, signal interference, the complexity of the wind field, and the limitations of the UAV itself, environmental factors, especially atmospheric conditions, also affect the accuracy and reliability of wind speed measurements. Atmospheric conditions, such as temperature, humidity, air pressure, and atmospheric stability, can directly impact wind speed measurements. For instance, unstable atmospheric conditions may lead to rapid changes in wind speed and direction, increasing the uncertainty of measurement data. Furthermore, the complexity of the wind field in urban building clusters, influenced by factors such as building layout, street orientation, and terrain, may also increase the uncertainty during the measurement process. The endurance and payload limitations, stability, and accuracy of UAVs are key factors affecting their ability to conduct long-duration and large-scale measurements. Therefore, when measuring wind speed, these environmental factors must be considered, and appropriate measures should be taken to reduce their impact on the measurement results.

Consequently, our research group has conducted a series of studies on the accuracy and reliability of UAV-based wind measurement systems. Consequently, our research group has conducted a series of studies on the accuracy and reliability of UAV-based wind measurement systems. Through preliminary wind tunnel experiments [31] and field measurement studies [32,33], the feasibility of the UAV-based wind measurement method has been verified. Additionally, our research group has also proposed a dual UAV wind measurement method. This method utilizes two UAV wind measurement

systems, with UAV A serving as the reference point and UAV B as the mobile measurement point. Through multiple measurements and calculations, the wind field conditions in the measured area can be effectively obtained. Using the dual UAV wind measurement method, our research group has successfully conducted measurement studies on wake wind fields of wind turbines [34] and flow around high-rise buildings [35].

### 2.1. Wind Tunnel Test

Wind tunnel method is used to modify the wind data collected by the UAV system. This wind tunnel has a 12 m test section with dimensions 3 m × 2.5 m, supporting speeds up to 20 m/s. Due to weak GPS reception inside, the UAV was not allowed to hover. Hence, we designed a 1 m stainless steel stand, securing the UAV with materials like tape. This design met tunnel blockage criteria (under 5%). The test setup is illustrated in Figure 2. For measurement accuracy, the SA210 and TFI Series 100 cobra probe were placed at an equal height.

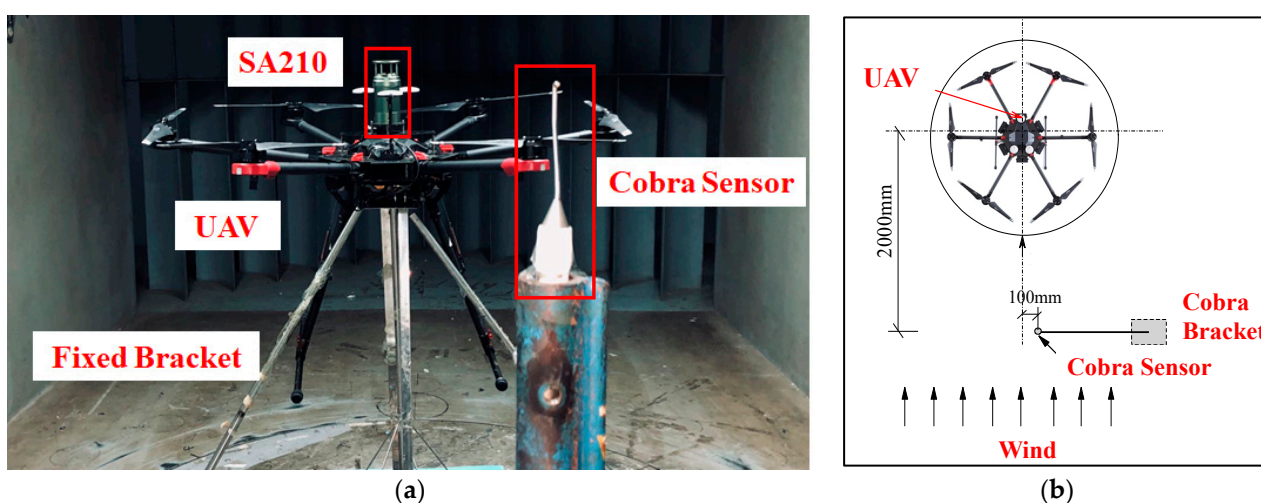


**Figure 2.** Wind Tunnel Measurement Diagram: (a) Actual Photo; (b) Top View Schematic.

When the UAV hovers in the air, it exhibits varying degrees of body posture adjustment to maintain precise positioning, depending on the incoming wind speed. The magnitude of the incoming wind speed is directly proportional to the angle of forward tilt of the UAV's body facing the incoming flow. Through wind tunnel experiments, the impact of the UAV's body posture adjustments and rotor rotation on the accuracy of the ultrasonic anemometer's wind measurement was analyzed and obtained. From the wind tunnel data, the UAV system recorded slightly elevated wind speeds compared to the cobra probe. To address this variance, a correction factor,  $\lambda$ , was introduced as per Equation (1). Table 2 shows  $\lambda$  values for different wind speed brackets. Post-correction, the UAV system's readings closely matched the cobra probe's data.

$$u(t) = u_w(t) / \lambda \quad (1)$$

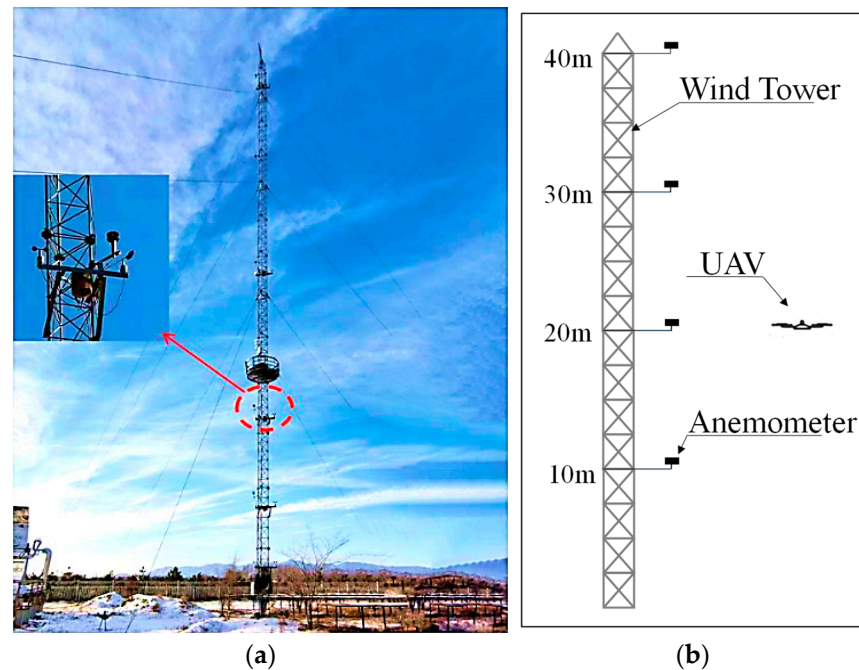
where  $u(t)$  denotes the corrected wind speed timeline from the UAV's body attitude, and  $u_w(t)$  is the uncorrected speed timeline captured by the UAV.

**Table 2.** UAV fuselage correction coefficient.

| Cobra (m/s) | [4–5) | [5–6) | [6–7) | [7–8) | [8–9) | [9–10) | [10–12) |
|-------------|-------|-------|-------|-------|-------|--------|---------|
| $\lambda$   | 1.005 | 1.011 | 1.016 | 1.021 | 1.032 | 1.044  | 1.075   |

## 2.2. Comparison between UAV-Based Wind Measurement System and Outdoor Wind Tower

Comparative outdoor experiments were conducted between the measurements from the UAV and a 40 m high wind tower [36]. The wind tower, as depicted in Figure 3a, was outfitted with a WindSonic ultrasonic anemometer at four specific altitudes: 10 m, 20 m, 30 m, and 40 m, and each of these instruments sampled at a frequency of 1 Hz. Meanwhile, the UAV was stationed 5 m horizontally from the wind tower, and it undertook measurements of the wind field at the aforementioned vertical heights, as demonstrated in Figure 3b.

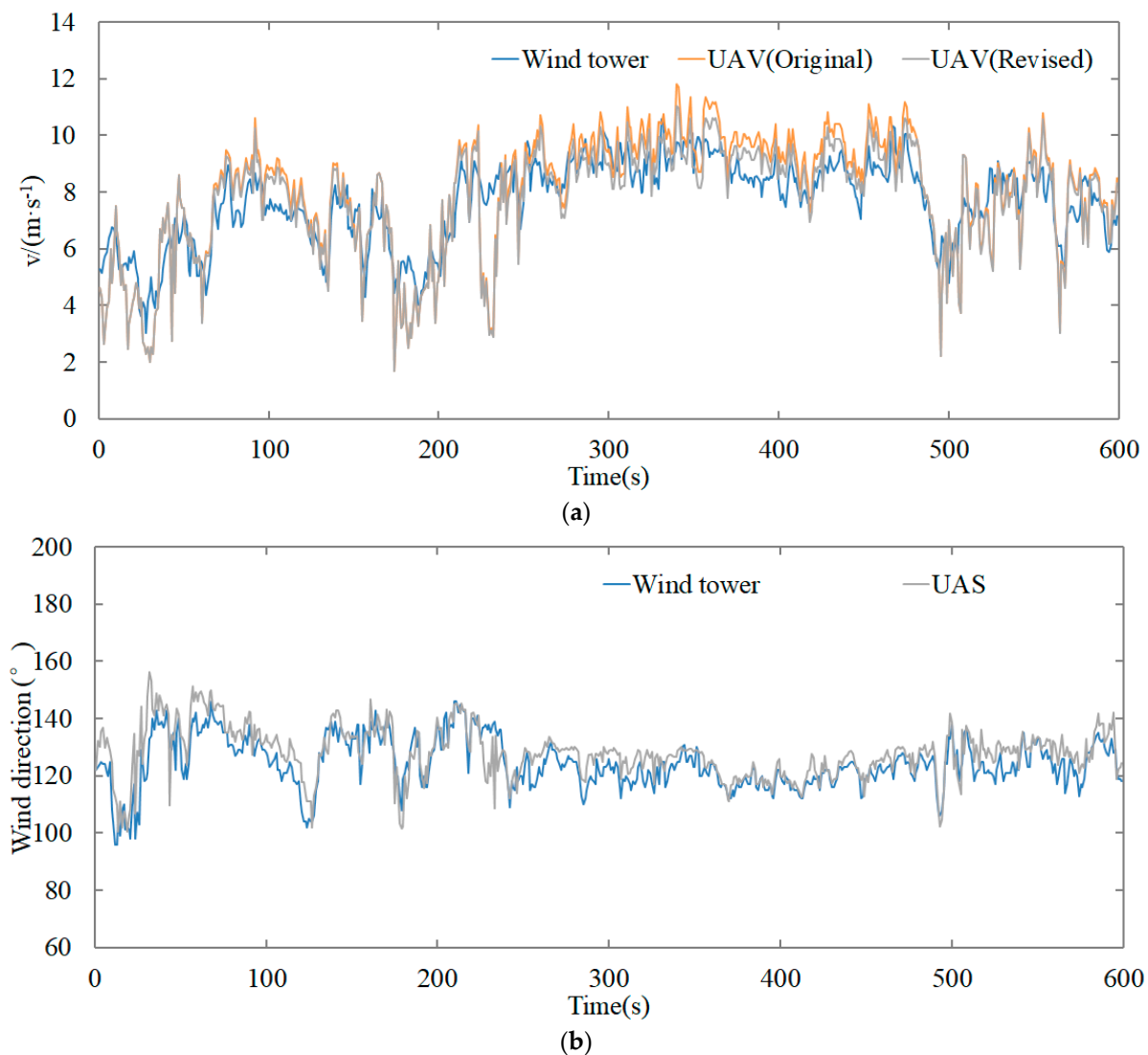


**Figure 3.** Wind Tower and UAV-based Wind Measurement System: (a) Wind Tower; (b) UAV Hovering Location Schematic.

Based on the measurement results, the original average wind speed measured by the UAV was slightly higher compared to the average wind speed measured by the wind tower. Upon analysis, it was found that the UAV exhibited varying degrees of forward tilt posture adjustments while hovering in the air when the wind speed changed. This caused some instantaneous wind field data obtained by the anemometer to have larger errors, increasing the fluctuation of the data. To minimize the impact of these factors on wind field measurements, a UAV body posture correction coefficient  $\lambda$  (as shown in Table 2) was used to correct the original data measured by the UAV. The corrected average wind speed profiles, wind direction angles, and turbulence results obtained by the UAV wind measurement system at heights of 10–40 m were compared with the results obtained by the wind tower anemometers at corresponding heights, as shown in Table 3. After correction, the data measured by the UAV wind measurement system had an error of less than 3% compared to the wind speed measurements at the corresponding heights of the wind tower, and the error in wind direction angles between the two was within 0.5% [37]. This indicates that the data correction method proposed in this paper can effectively calibrate the wind field data measured by the UAV-based system, making it more closely match the measurements of the wind tower. The time series of wind speeds from the wind tower and the UAV's original and corrected measurements are shown in Figure 4a, and the wind direction time series is shown in Figure 4b.

**Table 3.** Comparison of wind results between UAV and wind tower at different heights.

| Height | Mean Wind Speed |          |            | Mean Wind Direction |         |            | Mean Turbulence Intensity |       |            |
|--------|-----------------|----------|------------|---------------------|---------|------------|---------------------------|-------|------------|
|        | z/m             | UAV      | Wind Tower | Error               | UAV     | Wind Tower | Error                     | UAV   | Wind Tower |
| 10     | 7.23 m/s        | 7.15 m/s | 1.02%      | 237.02°             | 237.53° | 0.22%      | 0.172                     | 0.170 | 1.16%      |
| 20     | 7.35 m/s        | 7.30 m/s | 0.76%      | 242.59°             | 242.01° | 0.24%      | 0.143                     | 0.141 | 0.89%      |
| 30     | 8.28 m/s        | 8.30 m/s | 0.25%      | 243.28°             | 243.62° | 0.14%      | 0.136                     | 0.133 | 1.71%      |
| 40     | 8.86 m/s        | 8.93 m/s | 0.77%      | 243.46°             | 244.33° | 0.36%      | 0.130                     | 0.130 | 0.55%      |

**Figure 4.** Wind speed and wind direction timeline comparison [34]. (a) Wind speed; (b) Wind direction.

Upon examining the wind speed sequence graph from the wind tower, it becomes evident that during periods of consistent wind speed, the wind field sequences obtained by the UAV align with those of the wind tower. However, during periods of significant wind speed fluctuations (indicated by pronounced jagged patterns on the chart), the UAV's primary wind speed sequence exhibits increased volatility compared to that of the wind tower. This phenomenon is attributed to the UAV's need to adjust its posture to maintain precise hovering in gusty conditions, resulting in sporadic anemometer readings. After making corrections using the parameter  $\lambda$  and applying a moving average technique, the wind speed sequence from the UAV more accurately matches that of the wind tower.

From this analysis, it is evident that harnessing the precise positioning and hovering capabilities of the UAV can yield wind data from any specified location. We posit that

a hexacopter UAV equipped with an anemometer presents a promising approach for aerial wind field assessments. This approach emerges as a noteworthy enhancement to existing measurement methods, potentially addressing the limitations of traditional wind assessment techniques such as rigidity and high costs.

### 3. Measurement Site and Scheme

#### 3.1. Measurement Site

The experimental site is located in Taizhou City, Zhejiang Province, China, with the dominant wind direction in the wind farm being east wind. Five buildings with regular layouts in the urban area were selected as the measurement objects. Figure 5 shows a satellite image of the five buildings, and Figure 6 provides actual photos of Buildings 1# and 4#. From Figure 5, it can be observed that the wind measurement area is within the white dashed lines. Directly north of the measurement zone, Buildings 2# and 3# are situated, both adjacent to a 20 m tall structure. Additionally, to the western side of the measuring location, another building of the same height, 20 m, stands. Apart from these two buildings, there are no other obstructions in the area. Particularly, when the incoming wind direction is from the east, the measurement area is not obstructed by any tall buildings within a range of 1000 m in the wind direction. This provides an excellent research environment for the measurement and analysis of the wind field in the building cluster.



**Figure 5.** Top view of test site.

In the measured wind field area, the height of all five buildings is approximately 20 m, and there are trees with a height of around 10 m, as shown in Figure 6. All of these buildings have regular shapes. Specifically, Buildings 1# and 4# are cubes with a side length of 60 m. Building 3# is also a cube with a side length of 50 m. Building 2# and Building 5# have rectangular shapes, with respective side lengths of 70 m and 60 m.

During the measurement period, the wind direction was consistently eastward, as indicated by the blue arrows in Figure 5. Based on this wind direction, the buildings in the measurement area are organized into three rows and two columns. The first row includes Building 1# and Building 4#. The second row consists of Building 2# and Building 5#. The third row features only Building 3#. There are pedestrian pathways situated between the two columns of buildings, with a horizontal spacing of 35 m. Additionally, between the first and second rows of buildings, there is a landscaped pedestrian pathway with a horizontal

spacing of 50 m. Between the second and third rows of buildings, there is a pedestrian pathway with a width of 30 m.



**Figure 6.** Ground photo of the site.

### 3.2. Methodology for Gauging Incoming Wind Features

In field measurements, our focus is on comprehending the disruptions caused by incoming winds within the building cluster with the objective of capturing the dynamics of the flow field. To achieve this, we employed a dual UAV wind measurement approach to evaluate the relationship between wind speed and turbulence intensity at various aerial positions. This approach enabled us to monitor the fluctuations in both wind speed and turbulence intensity.

In the atmospheric boundary layer, the wind increases with height raised to the power of an alpha parameter (Equation (2)). This parameter has values between 0.15 and 0.40 depending on the roughness and atmospheric stability. This study employs two wind-measuring devices: UAV A and UAV B. Through repeated measurements, we determine the ratios of wind features across various locations. The scheme for assessing the vertical wind field at the site is outlined below:

The site designated for the wind field measurement is positioned 30 m downwind from the primary row of buildings (Buildings 1# and 4#), as illustrated in Figure 6. UAV A remains stationary at an altitude of 70 m, acting as the benchmark. In contrast, UAV B moves to 12 different altitudes, spanning from  $z = 10$  m to  $z = 120$  m. Each altitude is observed for a duration of 2 min. A crucial detail is the 15 m horizontal gap between the two UAVs. The trajectory linking the UAVs is orthogonal to the prevailing wind flow, depicted in Figure 7. After obtaining the wind speed measurement results from the two UAVs, the measured results for different wind speed segments were corrected based on the UAV fuselage correction coefficient  $\lambda$  to restore the wind speed time series results for UAV A and UAV B, respectively. Subsequently, by computing the wind speed ratios across these heights, the wind profile for any given moment  $t$  can be extrapolated by multiplying the wind speed value at the reference altitude [35].

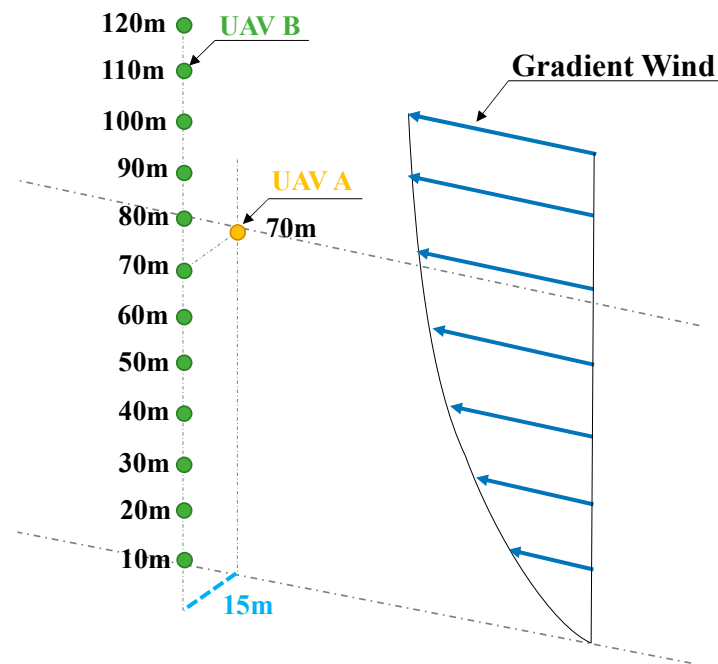


**Figure 7.** The dual UAV wind measurement method.

The characterization of the wind speed profile can be derived from Equation (2) [27]:

$$\frac{U_B}{U_A} = \left(\frac{z_B}{z_A}\right)^\alpha \quad (2)$$

where  $U_A$  is UAV A's corrected average wind speed at the reference height in m/s;  $U_B$  is the same for UAV B at varying heights.  $z_A$  is the hover height of UAV A, with a notable value of 70 m during testing, while  $z_B$  is UAV B's measurement height in meters.  $\alpha$  is termed as the roughness index [27].

The fundamental concept behind this methodology is to enhance the accuracy of describing and predicting variations in wind speed and turbulence within the atmosphere by comparing wind and turbulence data obtained from different UAVs. To improve the estimation of the turbulence intensity profile, it is combined with turbulence intensity data from a specific moment in time. Furthermore, these dimensionless ratios allow us to easily compare and integrate data from various locations and time points:

$$\lambda_U = \frac{U_B}{U_A} \quad (3)$$

$$\lambda_I = \frac{I_B}{I_A} \quad (4)$$

### 3.3. Measurement Scheme for Horizontal Wind Characteristics in the Building Cluster

To obtain the wind flow characteristics around the building cluster, the dual UAV wind measurement method is employed. Figure 8 presents the measurement coordinate plane for the horizontal wind field measurement. The coordinate axes are defined with the measurement point of Building 1# in the northeast direction as the origin (0, 0). The  $x$ -axis is parallel to the incoming wind direction, with positive values indicating downwind direction, ranging from  $x = 0$  to  $x = 280$  m. The  $y$ -axis is perpendicular to the incoming wind direction, pointing south as positive, ranging from  $y = 0$  to  $y = 175$  m. Therefore, there are a total of 130 measurement points in one height plane. For precise measurement, UAV A is used as a stable reference point to ensure accurate wind data. This UAV hovers at a specific location, 30 m horizontally in front of Building 1#, enabling it to better capture the

wind speed and direction in front of the structure. UAV B hovers within the wind field measurement area and performs point measurements at the coordinates shown in Figure 8. The measurement time for each coordinate point is 2 min.

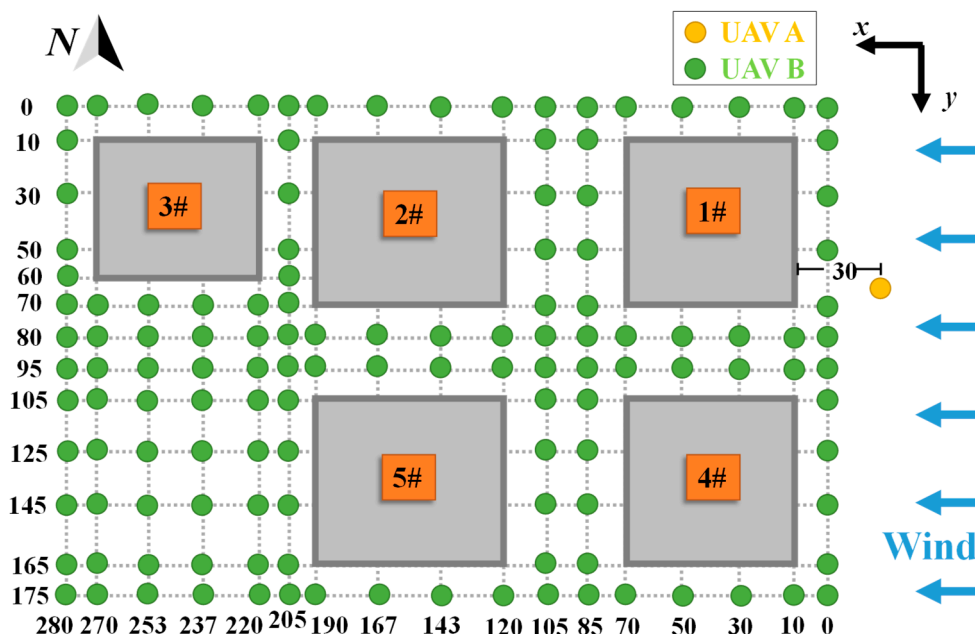


Figure 8. Coordinate plane diagram.

As shown in Figure 6, the heights of Buildings 1# to 5# are approximately 20 m, and the height of trees between the buildings is about 10 m. To ensure the safety of UAV operations and to conduct a comprehensive analysis of the wind field influenced by urban structures, we carried out measurements at two different heights. The surrounding trees reach a height of 10 m, necessitating that the UAV operates at a level well above this height to avoid collisions. Therefore, a height of 15 m ensures that the UAV safely flies above the trees, while also effectively measuring the wind field conditions within the height range of the buildings (20 m). Choosing a height of 25 m allows for the measurement of the flow field conditions beyond the height range covered by the buildings.

## 4. Results and Analysis

### 4.1. Incoming Wind Characteristics

During our observations, we observed that the wind consistently came from the east, maintaining a direction with an angle of  $90 \pm 8^\circ$  and an approximate speed of 7.5 m/s. Utilizing the methods we outlined earlier for assessing the wind field and turbulence intensity, we obtained data for the average wind speed and turbulence intensity within the 10–120 m range from the measurement point. These data are illustrated in Figure 9, representing just one set of our measurements.

To gain a deeper understanding of the data, we normalized the wind speed values for the 10–120 m range and fitted them to a wind profile. The result yielded  $\alpha = 0.2878$ , placing it between the type-C and type-D terrains as classified by the GB50009-2012 terrain classification. Further geographical analysis indicated that our measurement site is situated in an urban area densely populated with buildings on the east side and features terrain elevation ranging between 20–30 m, making it an ideal setting for our research.

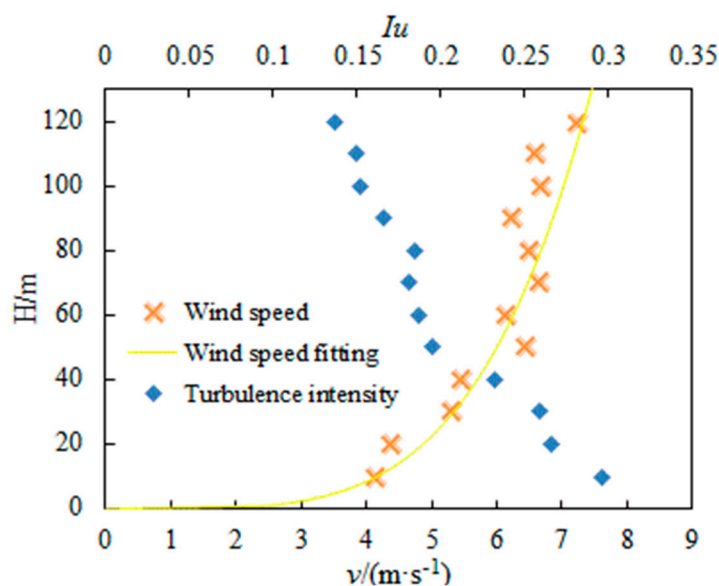


**Figure 9.** Measured wind speed and turbulence intensity (measured and fitted) vertical profiles at the inflow of the building cluster.

#### 4.2. Horizontal Wind Characteristics in Building Cluster

The measurement location is clearly depicted in Figure 10. Notably, the predominant wind direction forms a right angle with one side of the building cluster, offering a unique perspective for analyzing the wind's impact on the cluster. As the incoming wind traverses this group of structures, we can discern the flow characteristics around the buildings by scrutinizing changes in wind speed and turbulence intensity. To gain a deeper understanding of these shifts, we'll employ  $\lambda_U$  and  $\lambda_I$  to analyze the interplay between wind speed and turbulence and how they affect the building cluster.

During the field measurement, a large amount of wind speed and wind direction data related to the airflow around the buildings were obtained. Data from a time period with relatively small variations in wind speed (around 7.5 m/s) and wind direction ( $90 \pm 8^\circ$ ) were selected for the analysis of the building airflow, indicating a relatively stable wind speed variation. Given the square arrangement of the buildings, this relatively stable easterly wind direction was particularly crucial for analyzing the disturbances in the wind field between the buildings. Figure 11 displays the average wind speed and wind direction within a 2 min time interval at heights of 15 m and 25 m. It is evident from Figure 11 that within the inflow area of the buildings over this 2 min span, the average wind direction fluctuated between  $70^\circ$  and  $100^\circ$ . Notably, a significant portion of these wind direction changes were concentrated closely around  $90^\circ$ , specifically within a range of  $\pm 8^\circ$ . Within the 2 min time interval, the average wind speeds at the reference points of 15 m and 25 m mainly fell within the range of 4.6 m/s to 9.1 m/s and 4.7 m/s to 8.9 m/s, respectively. The average wind speeds at each height were approximately 6.0 m/s, and the mean turbulence intensities were approximately 0.28 and 0.25 for the 15 m and 25 m heights, respectively. In summary, the wind direction and wind speed remained relatively stable during the measurement period.



Figure 10. Field measurement photo of the UAV wind measurement system.

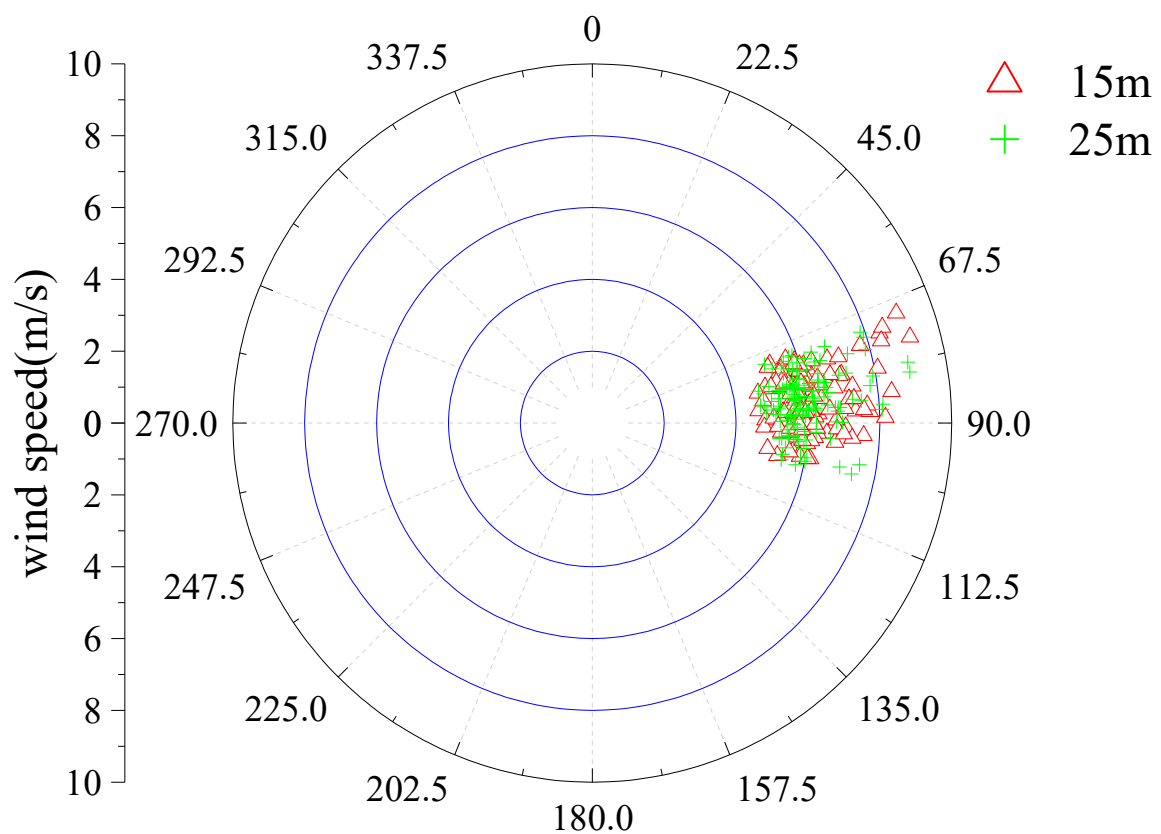


Figure 11. Field measurement image of the UAV-based wind measurement system.

Average Wind Speed

Figure 12 presents the  $\lambda_U$  within the measurement area.

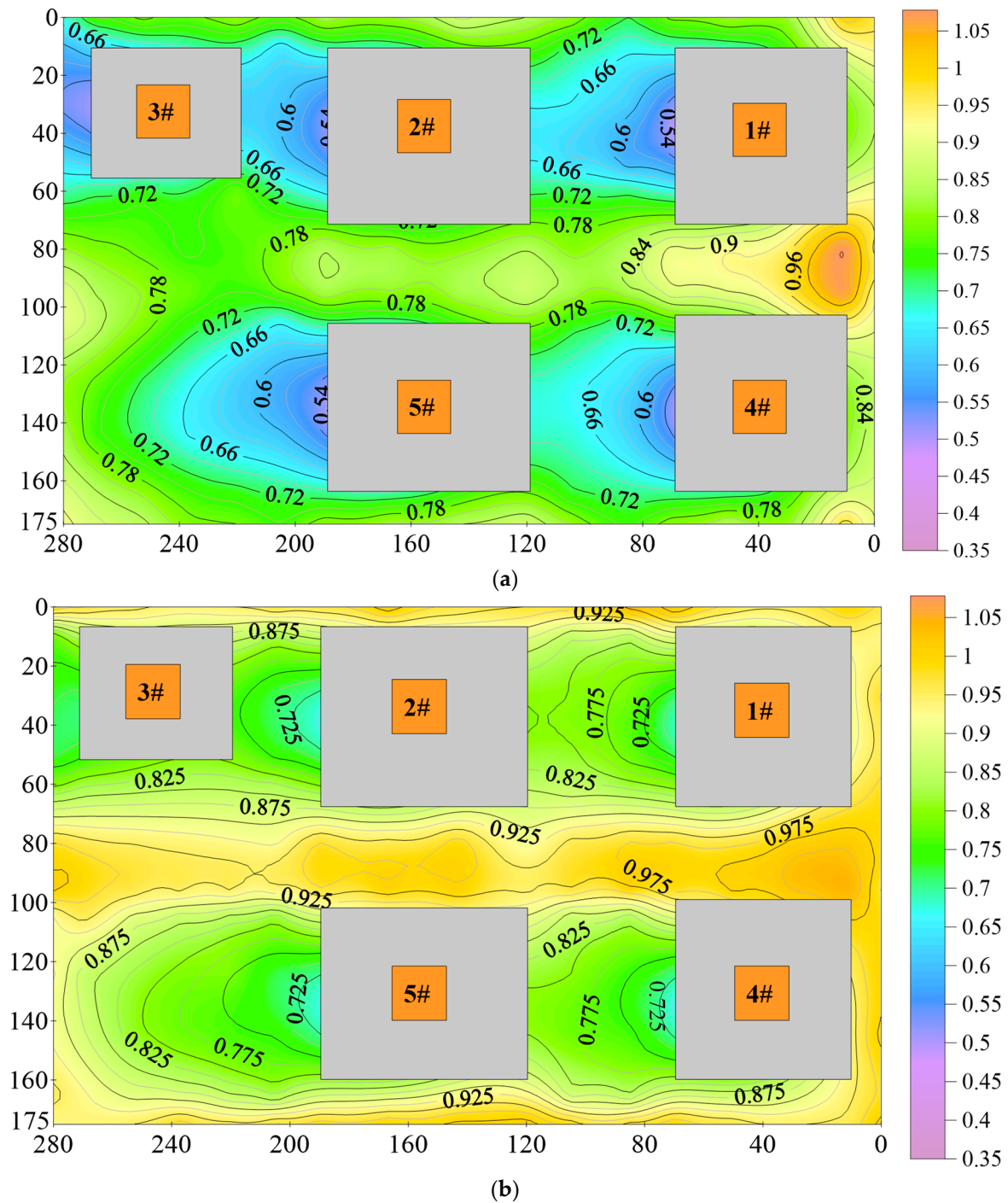


Figure 12. Contour map of wind speed ratio  $\lambda_U$  at different heights: (a) 15 m; (b) 25 m.

If the  $\lambda_U$  is around 1, it indicates that the wind speed is relatively close to the incoming flow velocity. As the  $\lambda_U$  decreases, the degree of wind speed reduction increases. From the above figure, it can be observed that the wind field between the buildings is generally complex. In terms of the interference effect of the wind field in the along-wind direction between the buildings, a “blocking effect” [38] is generally considered to exist in the case of serial arrangement. During the measurement period, according to the arrangement of the measured buildings shown in Figure 5, under the inflow wind direction, both the upstream and downstream buildings exhibit interference effects in the form of serial and parallel arrangements.

The  $\lambda_U$  in the lee side region of each building is relatively small, and it decreases as the distance to the building decreases. This indicates that the wind speed reduction on the lee side of the buildings is significant. Based on the wind field cloud map at a height of 15 m, it can be observed that the wind speed reduction is more pronounced at the rear of the buildings. For each building along its central axis, the wind speed ratios within a range of 10 m from the building are 0.49–0.55, within a range of 10–30 m are 0.55–0.62, and within a range of 30–60 m are 0.62–0.81. Furthermore, the wind speed reduction follows a trend of spreading towards both sides in the along-wind direction. The contour map of horizontal velocity distribution of buildings in the study by Zhou Chuanhui et al. [39] also exhibits a similar spreading trend, which is consistent with the results of the present measurement. Based on the wake flow of Building 5#, it is evident that the wind speed reduction caused by the building is more significant. According to the current measurement results, when the building height  $h = 20$  m, the length of the wake flow is greater than 4.5 times the building height, which is in agreement with the research findings of Zhengnong Li et al. [35].

In addition, although Buildings 2# and 3# have buildings in their inflow wind direction, the reduction in the wind speed wake regions of Buildings 2# and 3# is not more significant than that of Building 1#. This phenomenon differs from previous conclusions and deviates from the overall reduction pattern of the building complex in this measurement (which shows a stair-step reduction in the along-wind direction). It indicates that the narrow spaces between the buildings cause localized turbulence phenomena, leading to a more unstable regional wind field after the disturbance by the building complex. This finding aligns with the conclusions reached by researchers like Zhang Min et al. [40] through comprehensive numerical simulations and wind tunnel tests. Their research demonstrated that when buildings are arranged in a serial pattern, those positioned upfront exert a shielding or blocking effect on the structures behind. This blocking phenomenon is pivotal when studying wind direction and speed distribution within a building cluster since it can impact the wind load and overall stability of the structures. Compared to a height of 15 m, the wind speed contour map at a height of 25 m follows a similar pattern, with a lower degree of wind speed reduction. Thus, it can be concluded that buildings can affect the wind field in regions higher than the building height.

The wind field in the pedestrian passageway between the two rows of buildings is also subjected to varying degrees of interference. The length of the pedestrian passageway is 280 m, and overall, the  $\lambda_U$  is around 1. The location between Building 1# and Building 4# shows a relatively large wind speed ratio of approximately 1.03–1.1, indicating an increase in wind speed in this area. This is because the flow around the structure in a building complex is generally different from the flow around isolated buildings. A more intuitive example is the passageway located between the buildings, where the inflow wind disperses from both sides of the buildings and converges within the passageway, leading to a sharp increase in wind load and its response [37,41]. For parallel buildings such as Building 1# and Building 4#, and Building 2# and Building 5#, the side faces of the buildings are affected by the adjacent buildings, and the wind speed ratio in the pedestrian walkway gradually decreases. This is similar to the conclusion of Zhang Min et al. [40] and indicates that the interference mostly occurs on the side faces of adjacent buildings, with minimal impact on the windward faces of the adjacent buildings. At the intersection between Buildings 1#, 2#, 4#, and 5#, a slight increase in wind speed is observed. This is because the intersection is a wind-converging area, transforming from a sub-layer flow state to a fully turbulent state, resulting in an increase in wind speed. Compared to a height of 15 m, the wind speed contour map in the pedestrian passageway at a height of 25 m shows little variation, indicating that the interference effect between the two rows of buildings significantly decreases at greater heights than the building height.

Figure 13 presents the results of the turbulence intensity ratio  $\lambda_I$  within the measurement area.

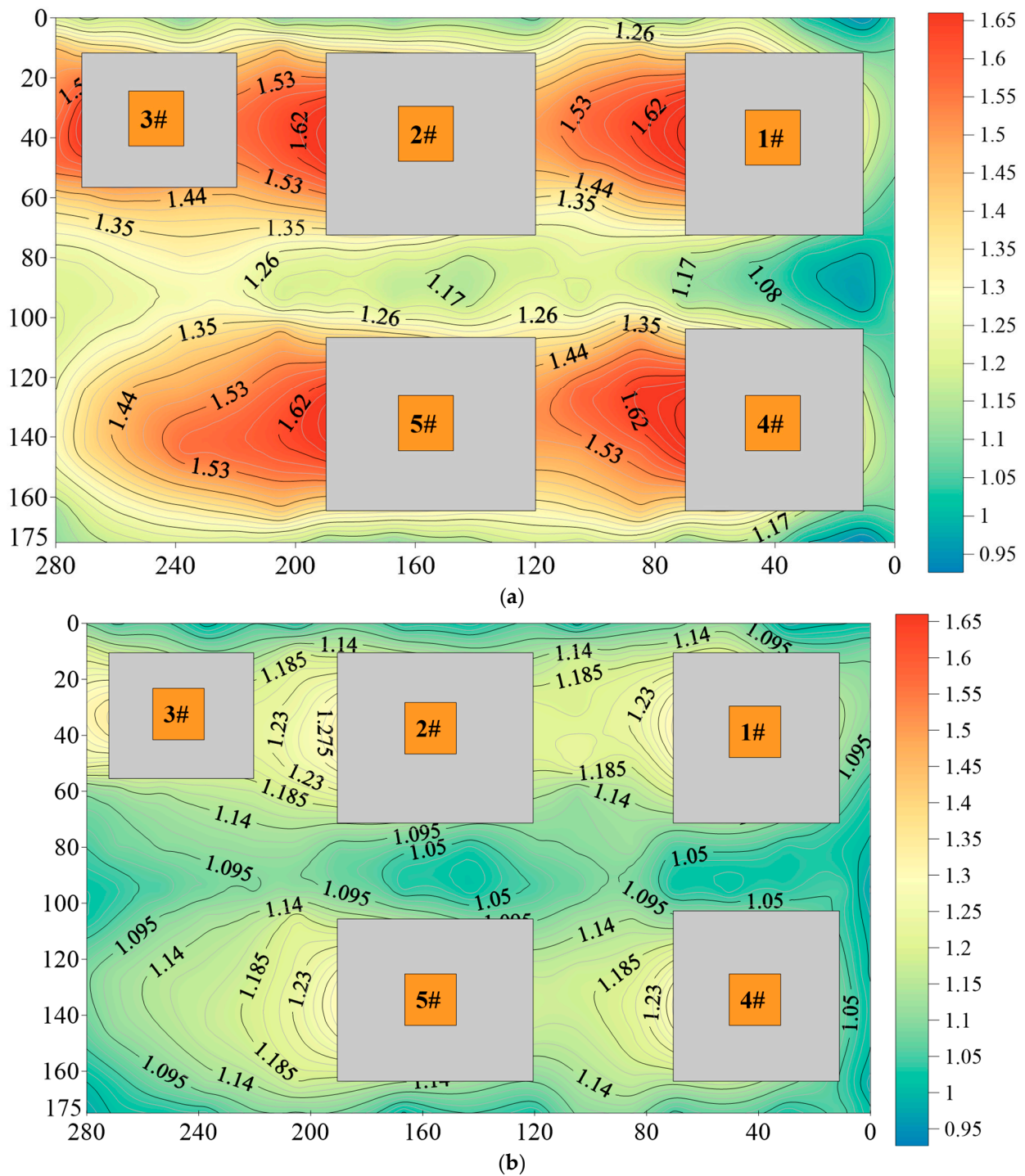


**Figure 13.** Contour map of turbulence intensity ratio  $\lambda_I$  at different heights: (a) 15 m; (b) 25 m.

From the above analysis, it is evident that turbulence intensity in the wake regions of the buildings results in a significantly non-uniform wind field structure. The overall pattern indicates that turbulence intensity increases with proximity to the buildings and on the leeward side axis of the shorter edges of the buildings.

Analyzing the contour map of turbulence intensity ratio  $\lambda_I$  at the 15 m plane reveals the following: at locations  $x = 5$  m,  $y = 30$  m, or  $y = 130$  m in the inflow region, turbulence intensity is higher compared to the inflow. This can be attributed to the local increase in turbulence caused by the impingement of the inflow wind on the eastern side of Building

1# or Building 4#. In the areas adjacent to the building walls, turbulence intensity ratios range between 1.2 and 1.3, indicating an increase in turbulence intensity. This suggests the occurrence of unstable wind fields in close proximity to the buildings, possibly involving separation and reattachment phenomena [36]. Regarding the wake regions, the turbulence intensity within each building's wake region is significantly higher compared to the inflow, with along-wind turbulence intensity ratios ranging from 1.5 to 1.75. The turbulence intensity is higher along the building's central axis and gradually decreases towards the sides, which is consistent with the findings of Shaofeng Nie et al. [42].

At the 25 m plane, the  $\lambda_I$  in the inflow region exhibit a more stable wind field compared to the 15 m plane. However, the wind field in the pedestrian passageway between the two rows of buildings remains unstable. This can be attributed to the inflow wind flow around the top and sides of the buildings, as this region is located at the junction where the wind field instability is amplified. In the wake regions, Buildings 1#, 2#, 3#, and 4# still experience an impact on turbulence intensity, with turbulence intensity ratios ranging from 1.2 to 1.3. Similarly, the wake turbulence intensity ratio  $\lambda_I$  for Building 5# ranges from 1.09 to 1.3. This suggests that even at heights higher than the buildings, the wind field can be affected by the top of the buildings, leading to increased turbulence due to vortex shedding or wind field disturbances. Based on the wake region of Building 5#, it can be inferred that the length of the wake flow exceeds 4.5 times the building height. Therefore, it is evident that the influence of buildings remains significant at the 25 m plane, and the flow patterns and turbulence intensity differ compared to the inflow.

## 5. Conclusions

Leveraging the UAV anemometry system, we conducted detailed measurements of the wind speed and turbulence intensity distribution within a building complex area, successfully capturing the wake wind field characteristics inherent to the zone. After meticulous research and data scrutiny, we derived the following conclusions:

- (1) Utilizing a dual UAV measurement strategy, we conducted precise assessments of wind speed and turbulence intensity spanning a 120 m range above the site. After data analysis, our fitting result indicated an  $\alpha$  value of 0.2878, which falls between the type-C and type-D terrains specified in the GB50009-2012 standard [27]. Importantly, this methodology offers significant advantages in terms of cost-effectiveness and operability, providing an efficient and economical means for outdoor wind field evaluations.
- (2) Wind field information at two height planes in the building complex flow field was obtained. The results indicate that the closer buildings are to each other, the more pronounced the attenuation (enhancement) effect on wind speed (turbulence intensity) of tall structures. The influence of the wake flow extends outward, and the wind speed reduction (turbulence intensity enhancement) is more prominent in the plane below the building height range. The wake wind field of buildings is significantly affected by nearby structures, and the length of the wake is greater than 4.5 times the building height.
- (3) When buildings are arranged in a serial manner, upstream buildings have a blocking effect on downstream buildings, indicating that the narrow spaces between buildings lead to localized turbulence phenomena, resulting in increased instability in the regional wind field after interaction with the building complex.
- (4) Wind speed (turbulence intensity) in the pedestrian passageway between the two rows of buildings exhibits significant enhancement (reduction). This is because the flow around structures in a building complex differs from that around isolated buildings. The incoming wind disperses from both sides of the windward faces of the buildings and converges within the passageway, leading to a sharp increase in wind load and its response.

**Author Contributions:** Conceptualization, O.P. and Z.L. (Zhengnong Li); methodology, B.Y.; software, T.B.; validation, T.B.; formal analysis, Z.C.; investigation, Z.C.; resources, L.Y. and H.Q.; data curation, O.P. and Z.L. (Zhen Li); writing—original draft preparation, O.P. and T.B.; writing—review and editing, O.P.; visualization, O.P.; supervision, Z.L. (Zhengnong Li); project administration, O.P.; funding acquisition, Z.L. (Zhengnong Li). All authors have read and agreed to the published version of the manuscript.

**Funding:** This research was supported by the National Natural Science Foundation of China (grant number 51278476); the Hainan Provincial Joint Project of Sanya Yazhou Bay Science and Technology City, China (grant number 2021CXLH0024); and the Key Research and Development Program of Hainan Province, China (grant number ZDYF2020207).

**Data Availability Statement:** The data that support the findings of this study are available from the corresponding author upon reasonable request. The data are not publicly available due to privacy.

**Acknowledgments:** We gratefully acknowledge the Key Laboratory of Building Safety and Energy Efficiency of the Ministry of Education Laboratory for providing the necessary wind tunnel test for this study.

**Conflicts of Interest:** Authors Ou Pu, Boqiu Yuan, Liwei Yang, Hua Qin and Zhen Li were employed by the company Guangxi Power Grid Co., Ltd. The remaining authors declare that the research was conducted in the absence of any commercial or financial relationships that could be construed as a potential conflict of interest.

## References

1. Shen, L.; Han, Y.; Tang, C.; Yuan, T.; Yang, Y.; Kuang, X. Study on wind tunnel test of wind environment under the influence of multiple factors. *Eng. Mech.* **2021**, *38*, 88–97.
2. Li, Z.; Sun, Z. How the surrounding multi-scale building clusters affect the wind loads of the super high-rise building. *ACE* **2023**, *26*, 1–19. [[CrossRef](#)]
3. Yu, X.F.; Xie, Z.N.; Zhu, J.B.; Gu, M. Interference effects on wind pressure distribution between two high-rise buildings. *J. Wind. Eng. Ind. Aerodyn.* **2015**, *142*, 188–197. [[CrossRef](#)]
4. Kim, W.; Tamura, Y.; Yoshida, A. Interference effects on local peak pressures between two buildings. *J. Wind. Eng. Ind. Aerodyn.* **2011**, *99*, 584–600. [[CrossRef](#)]
5. Mara, T.G.; Terry, B.K.; Ho, T.C.E.; Isyumov, N. Aerodynamic and peak response interference factors for an upstream square building of identical height. *J. Wind. Eng. Ind. Aerodyn.* **2014**, *133*, 200–210. [[CrossRef](#)]
6. Hui, Y.; Tamura, Y.; Yoshida, A. Mutual interference effects between two high-rise building models with different shapes on local peak pressure coefficients. *J. Wind. Eng. Ind. Aerodyn.* **2012**, *104*, 98–108. [[CrossRef](#)]
7. Zheng, Y.; Chen, S. Wind tunnel experimental study of Wind pressure distribution on tall buildings considering surrounding interference. In Proceedings of the 2011 International Conference on Consumer Electronics, Communications and Networks (CECNet), Xianning, China, 16–18 April 2011; pp. 5477–5480.
8. Xu, Z.; Yin, J. The Influence of Aeroelastic Effects on Wind Load and Wind-Induced Response of a Super-Tall Building: An Experimental Study. *Buildings* **2023**, *13*, 1871. [[CrossRef](#)]
9. Lavôr, T.F.A.; Brito, J.L.V.; Loredou-Souza, A.M. Interference effects mapping on the static wind loading of a tall building. *Lat. Am. J. Solids Struct.* **2023**, *20*, e484. [[CrossRef](#)]
10. Zhang, N.; Du, Y.; Miao, S.; Fang, X. Evaluation of a micro-scale wind model's performance over realistic building clusters using wind tunnel experiments. *Adv. Atmos. Sci.* **2016**, *33*, 969–978. [[CrossRef](#)]
11. Borraccino, A.; Schlipf, D.; Haizmann, F.; Wagner, R. Wind field reconstruction from nacelle-mounted lidar short-range measurements. *Wind. Energy Sci.* **2017**, *2*, 269–283. [[CrossRef](#)]
12. Zhou, Y.; Alam, M.M. Wake of two interacting circular cylinders: A review. *Int. J. Heat Fluid Flow* **2016**, *62*, 510–537. [[CrossRef](#)]
13. Lankadasu, A.; Vengadesan, S. Interference effect of two equal-sized square cylinders in tandem arrangement: With planar shear flow. *Int. J. Numer. Methods Fluids* **2008**, *57*, 1005–1021. [[CrossRef](#)]
14. Md, A.; Mahbub; Rehman, S.; Meyer, J.; Al-Hadhrami, L. Wind speed and power characteristics at different heights for a wind data collection tower in Saudi Arabia. In Proceedings of the World Renewable Energy Congress, Linköping, Sweden, 8–13 May 2011; pp. 4082–4089.
15. Sohankar, A. A LES study of the flow interference between tandem square cylinder pairs. *Theor. Comput. Fluid Dyn.* **2014**, *28*, 531–548. [[CrossRef](#)]
16. Sumner, D.; Richards, M.D.; Akosile, O.O. Two staggered circular cylinders of equal diameter in cross-flow. *J. Fluids Struct.* **2005**, *20*, 255–276. [[CrossRef](#)]
17. Li, Y.; Li, Q.S.; Ju, K.L. Experimental investigation of the wind pressure distribution and wind interference effects on a typical tall building. *Adv. Mater. Res.* **2013**, *639*, 444–451.

18. Huang, B.; Li, Z.; Zhao, Z.; Wu, H.; Zhou, H.; Cong, S. Near-ground impurity-free wind and wind-driven sand of photovoltaic power stations in a desert area. *J. Wind. Eng. Ind. Aerodyn.* **2018**, *179*, 483–502. [[CrossRef](#)]
19. Ren, Y.; Chen, S.; Yu, A.; Fan, M. Reliability Analysis of Wind Field and Boundary Layer Height in Xiamen Retrieved by Coherent Doppler Wind Lidar. *J. Arid. Meteorol.* **2021**, *39*, 514.
20. Ma, Q.; Li, Z.; Song, X.; Wu, S.; Li, R.; Tu, A. Observational study of low-level jet based on Doppler wind lidar. *J. Mar. Meteorol.* **2019**, *39*, 61–67.
21. Muschinski, A.; Frehlich, R.; Jensen, M.; Hugo, R.; Hoff, A.; Eaton, F. Fine-scale measurements of turbulence in the lower troposphere: An intercomparison between a kite-and balloon-borne, and a helicopter-borne measurement system. *Bound. Layer Meteorol.* **2001**, *98*, 219–250. [[CrossRef](#)]
22. Platis, A.; Siedersleben, S.K.; Bange, J.; Lampert, A.; Bärfuss, K.; Hankers, R.; Cañadillas, B.; Foreman, R.; Schulz-Stellenfleth, J.; Djath, B.; et al. First in situ evidence of wakes in the far field behind offshore wind farms. *Sci. Rep.* **2018**, *8*, 2163. [[CrossRef](#)]
23. Reuder, J.; Brisset, P.; Jonassen, M.; Müller, M.; Mayer, S. Sumo: A small unmanned meteorological observer for atmospheric boundary layer research/ /IOP Conference Series: Earth and Environmental Science. *IOP Publ.* **2008**, *1*, 012014.
24. Lawrence, D.A.; Balsley, B.B. High-resolution atmospheric sensing of multiple atmospheric variables using the DataHawk small airborne measurement system. *J. Atmos. Ocean. Technol.* **2013**, *30*, 2352–2366. [[CrossRef](#)]
25. Bruschi, P.; Piotto, M.; Dell’Agnello, F.; Ware, J.; Roy, N. Wind Speed and Direction Detection by Means of Solid-state Anemometers Embedded on Small Quadcopters. *Procedia Eng.* **2016**, *168*, 802–805. [[CrossRef](#)]
26. Zheng, J.; Wang, H.; Pei, B. UAV attitude measurement in the presence of wind disturbance. *Signal Image Video Process.* **2020**, *14*, 1517–1524. [[CrossRef](#)]
27. GB50009-2012; Load Code for the Design of Building Structures. China Architecture & Building Press: Beijing, China, 2012.
28. Prudden, S.; Fisher, A.; Marino, M.; Mohamed, A.; Watkins, S.; Wild, G. Measuring wind with small unmanned aircraft systems. *J. Wind. Eng. Ind. Aerodyn.* **2018**, *176*, 197–210. [[CrossRef](#)]
29. Prudden, S.; Watkins, S.; Fisher, A.; Mohamed, A. A flying anemometer quadrotor: Part 1. In Proceedings of the International Micro Air Vehicle Conference (IMAV 2016), Beijing, China, 17–21 October 2016; pp. 17–21.
30. Wetz, T.; Wildmann, N.; Beyrich, F. Distributed wind measurements with multiple quadrotor unmanned aerial vehicles in the atmospheric boundary layer. *Atmos. Meas. Tech.* **2021**, *14*, 3795–3814. [[CrossRef](#)]
31. Li, Z.; Hu, H.; Shen, Y. The influence of rotor rotation of hexacopter on wind measurement accuracy. *J. Exp. Fluid Mech.* **2019**, *33*, 7–14.
32. Li, Z.; Feng, H.; Pu, O.; Shen, Y. Research on boundary layer wind profile measurement based on six-rotor UAV anemometer. *Eng. Mech.* **2021**, *38*, 121–132.
33. Wu, H.; Zhang, L.; Feng, H.; Hu, H.; Li, Z. Wind field measurement over complex landforms based on multi-rotor nmanned aircraft. *J. Exp. Fluid Mech.* **2021**, *35*, 92–103.
34. Li, Z.; Pu, O.; Pan, Y.; Huang, B.; Zhao, Z.; Wu, H. A study on measuring wind turbine wake based on UAV anemometry system. *Sustain. Energy Technol. Assess.* **2022**, *53*, 102537. [[CrossRef](#)]
35. Li, Z.; Zhang, Z.; Pu, O.; Pan, Y.-Y.; Huang, B.; Shen, Y.-J.; Wu, H.-H. Measurement of flow around a typical building based on six-rotor UAV anemometer. *Eng. Mech.* **2022**, *40*, 151–160.
36. Zeng, J.; Li, M.; Zhang, Z.; Cao, B. Separation-Reattachment Flows Characteristics of Rectangular High-Rise Buildings with Different Side Ratios. *J. Southwest Jiaotong Univ.* **2020**, *55*, 780–788.
37. Mattias, L.W.A.; Paramo, C.A.M. Study of the dynamic response of a CAARC building by the synthetic wind method and comparison with different approaches. *Multidiscip. Model. Mater. Struct.* **2022**, *18*, 142–152. [[CrossRef](#)]
38. English, E.C. Shielding factors from wind-tunnel studies of prismatic structures. *J. Wind. Eng. Ind. Aerodyn.* **1990**, *36*, 611–619. [[CrossRef](#)]
39. Zhou, C. Relation Between the Zone of Aerodynamic Shadow and the External Dimensions of Building. *Build. Energy Environ.* **2003**, *4*, 49–51.
40. Zhang, M.; Lou, W.-J.; He, G.-J.; Shen, G.-H. Numerical study on interference effects of wind loads about a cluster of tall buildings. *Eng. Mech.* **2008**, *25*, 179–185. [[CrossRef](#)]
41. Wang, X.; Jia, B.; Ge, X. Comparative study on wind load coefficients of ultra large container ship in different loaded conditions. In Proceedings of the 2019 Chinese Automation Congress (CAC), Hangzhou, China, 22–24 November 2019; pp. 5016–5021.
42. Nie, S.; Zhou, X.; Zhou, T.; Shi, Y. Numerical Simulation of 3D Atmospheric Flow Around a Bluff Body of CAARC Standard High-Rise Building Model. *J. Civ. Environ. Eng.* **2009**, *31*, 40–46.

**Disclaimer/Publisher’s Note:** The statements, opinions and data contained in all publications are solely those of the individual author(s) and contributor(s) and not of MDPI and/or the editor(s). MDPI and/or the editor(s) disclaim responsibility for any injury to people or property resulting from any ideas, methods, instructions or products referred to in the content.